Magnetic Nanorotors with Tailored Field-Induced Dynamics

Mathias Feyen,[†,‡] Erik Heim,[§] Frank Ludwig,[§] and Annette M. Schmidt*,[†]

Institut für Organische Chemie und Makromolekulare Chemie, Heinrich-Heine-Universität Düsseldorf, D-40225 Düsseldorf, Germany, and Institut für Elektrische Messtechnik und Grundlagen der Elektrotechnik, Technische Universität Carolo-Wilhelmina zu Braunschweig, D-38106 Braunschweig, Germany

Received December 2, 2007. Revised Manuscript Received February 8, 2008

Electromagnetically induced nanoparticle rotation controlled by hydrodynamics and by the frequency of the applied field is observed for the presented system of monodomain magnetic core−shell hybrids. The system is composed of nanoscopic cobalt cores decorated with a poly(ε-caprolactone) brush shell with adjustable thickness, immersed in toluene. By using alternating current (AC) susceptometry and magnetic heating calorimetry, a clear dependence of the dynamic magnetic behavior on the shell thickness is observed at constant core properties, that may be of use for microfluidic transport applications.

Introduction

Ongoing miniaturization of electronic and electomechanical devices has a steady impact on many areas of everyday life, such as computers, communication devices, manufacturing, and transportation. However, existing concepts for microelectromechanical systems (MEMS) approach their limits due to dominant surface effects and thermoelastic damping on the nanoscale,[1] giving rise to the development of alternative actuation concepts toward meso-, nano-, and even molecular scale systems that are able to convert various forms of energy (chemical, electromagnetical, electrochemical) into kinetic movement.[2]

Here, nature often serves as a powerful example for highly effective and specific, locally operating molecular machines. Motor proteins like kinesins, myosins, and dynesins are operated by the hydrolysis of ATP. The associated chemical energy is converted into the desired mechanical output, e.g., signal transduction, intracellular trafficking, and locomotion of cellular components.[3] A key feature is the asymmetry implied in the molecular and hierarchical design which allows the locally available energy to be expended in directed mechanical forces. On this basis, biomimetic molecular motor systems have been designed and applied to nanoscaled objects.[4]

The challenges of this subject arise from the small object size and its high surface-to-volume ratio. As a consequence, (random) thermal motion already impacts the motion dynamics,[5] and the operation is dominated by low Reynolds number hydrodynamics.[6]

Driving forces for nanomotors include the gradients in dissipative systems,[3] that may be of thermal or concentration nature, field gradients (electro- and magnetophoresis), and chemical,[7,8] optical,[9,10] or electrical activation.[1,11]

Although the majority of studies described have focused on molecular systems in solution, recent reports on crystalline molecular[12,13] and nanoscale rotors[1,3,7] have addressed pertinent questions on speed, friction, and potential wear in different environments. Although the direction of the motion in these systems is random, they demonstrate how control over rotary motion might be realized. In an ideal case, the nano-objects would be compelled by the applied electromagnetic field to rotate by a predetermined, dynamically controlled angle while other objects and molecules in the system would not be affected by these fields.

An alternative concept for the rotational activation of nano-objects is based on the reorientation of permanent or induced dipoles by an appropriate stimulus. In alternating fields, nanoparticles possessing an electrical or magnetic dipole (e.g., metallic, monodomain liquid crystalline or magnetic nanoparticles) undergo a reversal of their moment driven by the rotation of the field vector. Concerning single-domain magnetic nanoparticles (MNP), the magnetization reversal can principally occur by two mechanisms.[14] For particles

* Corresponding author. E-mail: schmidt.annette@uni-duesseldorf.de.
† Heinrich-Heine-Universität Düsseldorf.
‡ Present adress: Max-Planck-Institut für Kohlenforschung, D-45470 Mülheim a. d. Ruhr, Germany.
§ Technische Universität Braunschweig.

(1) Fennimore, A. M.; Yuzvinsky, T. D.; Han, W.-Q.; Fuhrer, M. S.; Cumings, J.; Zettl, A. *Nature* **2003**, *424*, 408.
(2) Browne, W. R.; Feringa, B. L. *Nat. Nanotechnol.* **2006**, *1*, 25.
(3) Paxton, W. F.; Sundararajan, S.; Mallouk, T. E.; Sen, A. *Angew. Chem., Int. Ed.* **2006**, *45*, 5420.
(4) Cameron, L. A.; Footer, M. J.; van Oudenhaarden, A.; Theriot, J. A. *Proc. Natl. Acad. Sci. USA* **1999**, *96*, 4908.
(5) Astumian, R. D. *Science* **1997**, *276*, 917.
(6) Purcell, E. M. *Am. J. Phys.* **1976**, *45*, 3.
(7) Paxton, W. F.; Kistler, K. C.; Olmeda, C. C.; Sen, A.; St, S. K.; Cao, Y.; Mallouk, T. E.; Lammert, P. E.; Crespi, V. H. *J. Am. Chem. Soc.* **2004**, *126*, 13424.
(8) Fournier-Bidoz, S.; Arsenault, A. C.; Manners, I.; Ozin, G. A. *Chem. Commun.* **2005**, 441.
(9) Khan, M.; Sood, A. K.; Deepak, F. L.; Rao, C. N. R. *J. Nanosci. Nanotechnol.* **2007**, *7*, 1800.
(10) Stockmann, M. I.; Li, K.; Brasselet, S.; Zyss, J. *Chem. Phys. Lett.* **2006**, *433*, 130.
(11) Král, P.; Seideman, T. *J. Chem. Phys.* **2005**, *123*, 184702.
(12) Garcia-Garibay, M. A. *Proc. Natl. Acad. Sci.* **2005**, *102*, 10771.
(13) Khuong, T.-A.; Zepeda, G.; Ruiz, R.; Khan, S. I.; Garcia-Garibay, M. A. *Cryst. Growth Des.* **2004**, *4*, 15.
(14) Fannin, P. C. *Adv. Chem. Phys.* **1998**, *104*, 181.

10.1021/cm703419t CCC: $40.75
Published on Web 04/08/2008

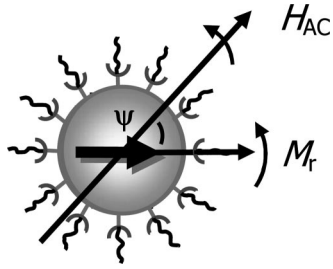

Figure 1. Diffusive rotation of a blocked MNP in an alternating current (AC) electromagnetic field.

with a low anisotropy barrier, e.g. in iron oxides with a diameter around 10 nm, the magnetic dipole moment rapidly rotates inside the particles due to thermal or magnetic activation (Néel reversal). On the other hand, cobalt nanoparticles of the same size (or bigger iron oxide particles) possess an anisotropy barrier that is orders of magnitude higher than thermal energy, thus resulting in blocking behavior of the magnetic dipole moment in the crystal lattice of the particle. As a consequence, such systems are forced to a fast, Brownian-like rotation of the whole particle in alternating fields (Figure 1). As such, the characteristic time scale of such a process, represented by the Brownian relaxation time τ_B depends on the hydrodynamic volume V_h of the particles and the viscosity η of the system (eq 1):[15,16]

$$\tau_B = \frac{3V_h\eta}{k_B T} \quad (1)$$

with k_B being Bolzmann's constant, and T, the temperature, respectively. Thus, in suitable magnetic particle dispersions, the energy of the time-dependent field is partially transformed into kinetic energy of the particles. The internal rotation, meaning the rotation of the particles relative to the surrounding fluid, causes imposing effects such as entrainment of the fluid by the field.[17] At the same time, the particles can be locally manipulated using superimposed inhomogeneous direct current (DC) magnetic fields.[19]

Thus, during the past few years, increasing attention has been drawn to the dynamic properties of blocked single-domain magnetic particles, giving rise to sophisticated concepts for field-induced particle rotation and magnetic heating.[18,19] In some recent studies, based on AC susceptometry,[20–22] magnetorheometry,[18] and ferromagnetic relaxation methods,[23] the relation between the Brownian relaxation time τ_B, the hydrodynamic particle volume V_h, and solvent viscosity η in ferrofluids of blocked magnetic single-domain particles is clearly shown and is attributed to a field-induced particle rotation with the time constant τ_B. The unique ability of magnetic nanoparticles to convert magnetic energy into mechanical rotation in dynamic magnetic fields is of high interest for laboratory-on-a-chip applications,[24] tumor therapy,[25] amplified DNA sensing,[26] magnetically activated drug delivery,[27] and bioelectrocatalytic systems.[18,26] In particular, AC susceptometry has been proposed[28,29] and experimentally shown[30] to be an adequate method to prove and quantitatively analyze the binding of biologically relevant molecules to functional magnetic nanoparticles for sensor systems and assays. Particle-rotation-induced flow is directly observed on a macroscopic scale,[17] and its implication in microfluidic devices has been demonstrated.[24]

However, the role of a hydrodynamic stabilizing shell as a simple tool to modify dynamic properties and thus the rotational speed of blocked MNPs has yet to be highlighted. In this work, we demonstrate that by the decoration of magnetic nanoparticles with a polymer brush shell of variable thickness[31] it is possible to tailor the characteristic rotation frequency of dispersed particles, thus opening the possibility to address particle species independently without affecting the magnetic characteristics of the core. We report the impact of the shell thickness on the rotational diffusion of the hybrid particles in an oscillating magnetic field by careful analysis of AC susceptometry experiments and of magnetic heating characteristics.

Experimental Section

All synthetic procedures were performed under argon atmosphere.

Synthesis of Cobalt Nanoparticles. The cobalt particles have been synthesized by thermal decomposition of dicobaltoctacarbonyl $Co_2(CO)_8$ by a method according to Bönnemann et al.[39] and received as a powder. In a second step, the particles were stabilized by ultrasonic radiation in the presence of ricinolic acid, followed by repeated washing cycles in ethanol in order to remove excess surfactant, and redispersed in toluene.

Surface-Initiated Ring Opening Polymerization of ε-Caprolactone. Ricinolic acid functional Co particles dispersed in toluene are placed in a two-neck flask, and the required amount of ε-caprolactone and tin(II)-bis(2-ethylhexanoate) as the catalyst was added. Afterward, the mixture is heated to 130 °C and polymerized for 5 h. After cooling to room temperature, the particles are purified by precipitation in hexane and redispersion in toluene, followed by dropwise addition of ethanol at 0 °C and magnetic separation of the precipitated particles in order to remove free polymer chains.

Acidolysis of Co Cores. In order to characterize the polymer arms, Co cores are dissolved by addition of 6 M hydrochloric acid and stirred, until the black color disappears and a bluish aqueous

(15) Einstein, A. *Investigations on the Theory of Brownian Movement*; Dover: New York, 1956; pp 32−33.
(16) Frenkel, J. *Kinetic Theory of Liquids*; Dover: New York, 1955; p 251.
(17) Krauβ, R.; Liu, M.; Reimann, B.; Richter, R.; Rehberg, I. *New J. Phys.* **2006**, *8*, 18.
(18) Gazeau, F.; Baravian, C.; Bacri, J.-C.; Perzynski, R.; Shliomis, M. I. *Phys. Rev. E* **1997**, *56*, 614.
(19) Zahn, M. *J. Nanopart. Res.* **2001**, *3*, 73.
(20) Fischer, B.; Huke, B.; Lücke, M.; Hempelmann, R. *J. Magn. Magn. Mater.* **2005**, *289*, 74–77.
(21) Goya, G. F.; Fernandez-Pachero, R.; Arruebo, M.; Cassinelli, N.; Ibarra, M. R. *J. Magn. Magn. Mater.* **2007**, *316*, 132–135.
(22) Bao, Y.; Pakhomov, A. B.; Krishan, K. M. *J. Appl. Phys.* **2006**, *99*, 08H107/1–08H107/3.
(23) Malaescu, I.; Marin, C. N. *Physica B Condens. Matter* **2005**, *365*, 134–140.
(24) Gijs, M. *Microfluid. Nanofluid.* **2004**, *1*, 22.
(25) Jordan, A.; et al. In *Scientific and Clinical Applications on Magnetic Carriers*; Hafeli, U., Schutt, W., Teller, J., Zborowski, M., Eds.; Plenum: New York, 1997; pp 569−565.
(26) Weizmann, Y.; Patolsky, F.; Katz, E.; Willner, I. *J. Am. Chem. Soc.* **2003**, *125*, 3452.
(27) Häfeli, U. *Intern. J. Pharmaceut.* **2004**, *277*, 19.
(28) Connolly, J.; St, T. G. *J. Magn. Magn. Mater.* **2001**, *225*, 156–160.
(29) Nutting, J.; Antony, J.; Meyer, D.; Sharma, A.; Qiang, Y. *J. Appl. Phys.* **2006**, *99*, 08B319/1–08B319/3.
(30) Chung, S. H.; Hoffmann, A.; Bader, S. D.; Liu, C.; Kay, B.; Makowski, L.; Chen, L. *Appl. Phys. Lett.* **2004**, *85*, 2971–2973.
(31) Feyen, M.; Mattoussevitch, N.; Behrens, S.; Kolb, U. Schmidt, A. M., *Polymer*, submitted for publication.

phase can be separated from the organic, polymer-containing phase. The aqueous phase is washed with toluene, and the organic fractions with 1 M hydrochloric acid, brine, and water. The polymer is obtained by drying the organic phase in vacuo and is analyzed with ^{1}H NMR, attenuated total reflectance infrared red (ATR-IR), and gel permeation chromatography (GPC).

Thermogravimetric Analysis (TGA). The cobalt content of dry hybrid particles is investigated by TGA on a Netsch STA 449C Jupiter at a constant heating rate of 10 K·min^{-1} in helium atmosphere between 30 and 600 °C. The solid residues at 600 °C are attributed to the inorganic component.

Elemental Analysis (EA). The content of organic material (based on carbon content) can be extracted from EA based on a Perkin-Elmer ACHN analyzer 2004 with an accuracy of 0.3%.

Gel Permeation Chromatography (GPC). After hydrolysis of the core with aqueous HCl, the polymeric fraction is precipitated in hexane and investigated by GPC. The system setup is composed of a Waters 510 pump, an SFD autosampler, three polystyrene-based columns with a pore size between 100 and 10 000 Å, and a Waters differential refractometer. Experiments are conducted in THF at 1 mL·min^{-1} at ambient temperature, relative to PS standards.

Atomic Force Microscopy (AFM). The particles were visualized by AFM technique immersed in Xylene absorbed on a mica wafer on a MFP-3D (Asylum Research) with a TR400 Si3N4 cantilever (Olympus).

Transmission Electron Microscopy (TEM). TEM images of dropcast and dried samples from toluene on carbon-coated copper grid 400 were obtained from a Philips Tecnai F20 with an acceleration voltage of 200 kV.

Dynamic Light Scattering (DLS). The hydrodynamic diameter of Co@RA (ricinolic acid) and Co@PCL (poly(ε-caprolactone)) samples dispersed in toluene was evaluated using a High Performance Particle Sizer HPP5002 (Malvern Instruments), and analysis was conducted with the integrated software.

The viscosity of the investigated fluid was analyzed by flow viscosimetry at 25 °C in an Ostwald viscosimeter with a flow volume of 0.5 mL and a capillary diameter of 0.3 mm.

Vibrating Sample Magnetometry (VSM). Quasi-static magnetic properties of the samples were performed on a MicroMag vibrating sample magnetometer from Princeton Measurements Corporation, with a field maximum of 1.3×10^6 A·m^{-1}.

AC susceptometry measurements were performed with a home-built susceptometer similar to conventional differential systems. The maximum field amplitude is 0.25 mT and the maximum excitation frequency is 40 kHz, limited by the coil characteristics.

Magnetic heating experiments were conducted on a Hüttinger High Frequency Generator TIG 5, 0/300 equipped with a copper inductor ($l = 50$ mm, $d_I = 35$ mm, $n = 5$) and operating at 300 kHz. The maximum induction power was 5.0 kW.

Results and Discussion

Cobalt nanoparticles with a tailored hydrodynamic radius at constant core properties were synthesized by surface-initiated ring-opening polymerization[32–35] as a versatile method for the preparation of polymer brush shells of high

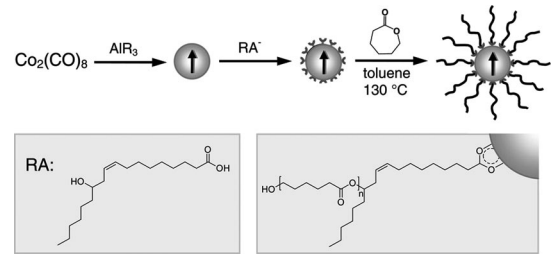

Figure 2. Pathway employed for the synthesis of Co@PCL core−shell particles with variant shell thickness. RA: ricinolic acid.

grafting density and adjustable thickness, as has recently been shown for ferrite particles.[31,36–38] The three-step synthetic pathway is sketched in Figure 2. Cobalt core particles with a diameter of 10 nm are obtained by thermolysis of $Co_2(CO)_8$ in the presence of aluminum alkyls and subsequent smooth oxidation.[39] They were surface-functionalized with ricinolic acid by chemisorption of the carboxylic acid group in order to introduce hydroxyl groups that serve as the initiators for the ring-opening polymerization of ε-caprolactone in the last step, resulting in the creation of a poly(ε-caprolactone) brush on the particle surface, with a high degree of synthetic flexibility concerning composition and thickness of the shell.[31] By choice of the particle-to-monomer ratio, the arm length of the polymer brush shell can be tailored and thus the hydrodynamic radius is influenced.

In this study, cobalt nanoparticles of a single synthetic batch, and decorated with polymeric brush shells of variable thickness, are analyzed with respect to the core properties by magnetic measurements and by dynamic light scattering (DLS) in order to compare the diffusive properties to AC susceptometry results.

Information on the cobalt content of the dry hybrid particles is gained by thermogravimetric analysis (TGA), while the molecular weight of the polymeric arms is accessed by gel permeation chromatography (GPC) after acidolysis of the core. The results are summarized in Table 1. ATR-FTIR confirms the presence of PCL in all samples.

A linear increase in the molar mass of the isolated polymer arms with growing polymer-to-cobalt ratio of the hybrids is detected by GPC. The result is in accordance with the assumption of a constant grafting density of chains on the particle surface. In all cases, the polydispersity index concerning the polymer chain length is close to 2, as commonly observed for poly(ε-caprolactone)s obtained by ring-opening polymerization.

The grafting density f_s can be calculated from the slope of the graph of M_n vs the polymer-to-cobalt ratio μ_{PCL}/μ_{Co} by using

$$f_s = \frac{\mu_{PCL}}{\mu_{Co}} \cdot \frac{1}{M_n} \qquad (2)$$

resulting in a value of (0.22 ± 0.02) mmol·g^{-1} with respect to the cobalt cores. Taking into account an average particle

(32) Lahann, J.; Langer, R. *Macromol. Rapid Commun.* **2001**, *22*, 968.
(33) Möller, M.; Nederberg, F.; Lim, L. S.; Kange, R.; Hawker, C. J.; Hedrick, J. L.; Gu, Y. D.; Shah, R.; Abbott, N. L. *J. Polym. Sci., Part A: Polym. Chem.* **2001**, *39*, 3529.
(34) Choi, I. S.; Langer, R. *Macromolecules* **2001**, *34*, 5361.
(35) Husemann, M.; Mecerreyes, D.; Hawker, C. J.; Hedrick, L. J.; Shah, R.; Abbott, N. L. *Angew. Chem., Int. Ed.* **1999**, *38*, 647.
(36) Schmidt, A. M. *Macromol. Rapid Commun.* **2005**, *26*, 93.
(37) von Werne, T.; Patten, T. E. *J. Am. Chem. Soc.* **2001**, *123*, 7497.
(38) Lattuada, M.; Hatton, T. A. *Langmuir* **2007**, *23*, 2158.
(39) Bönnemann, H.; Brijoux, W.; Brinkmann, R.; Matoussevitch, N.; Waldöfner, N.; Palina, N.; Modrow, H. *Inorg. Chim. Acta* **2003**, *350*, 617.

Table 1. Composition and Quasi-static Magnetic Properties of the Hybrid Co@RA and Co@PCL Core−Shell Particles and Their Dispersions in Toluene

run[a,b]	$\mu_{Co,dry}$[c] (mass-%)	d_v (nm)	M_n (g·mol^{-1})	M_s (kA·m^{-1})	$\mu_{Co,disp}$ (mass-%)	χ_{ini}	m_v ($\times 10^{-19}$ A·m^2)	d^c (nm)
Co@RA	87.3[c]	17.2	nd	0.47	0.31	0.03	7.29	9.8
Co@PCL13	39.7	22.1	1300	nd	nd	nd	nd	nd
Co@PCL17	28.1	25.2	1700	1.20	0.90	0.09	7.44	9.9
Co@PCL23	23.0	26.3	2300	2.06	1.58	0.16	7.85	10.1
Co@PCL27	18.5	30.9	2700	2.88	1.97	0.22	7.65	10.0
Co@PCL32	13.7	38.5	3200	3.71	2.83	0.28	7.33	9.9

[a] $\mu_{Co,dry}$: cobalt mass content of dry particles, from TGA. d_v: volume-average hydrodynamic diameter, from DLS. M_n: number-average molar mass of polymer arms, from GPC. M_s: saturation magnetization. $\mu_{Co,disp}$: cobalt mass content of dispersions; χ_{ini}: initial susceptibility. m_v: volume average magnetic moment of the cobalt core. d_c: core diameter, from VSM. [b] Nomenclature: Co@RA, ricinolic acid functionalized cobalt nanoparticles. Co@PCL*xy*, cobalt nanoparticles with poly(ε-caprolactone) brush shell. $xy = M_n/100$. nd, not determined. [c] By elemental analysis (C content).

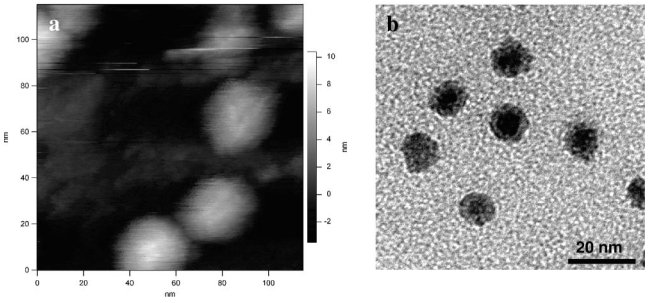

Figure 3. (a) AFM and (b) TEM images of Co@PCL27 core−shell particles.

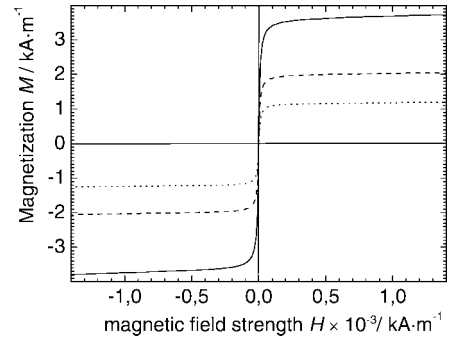

Figure 4. Quasi-static magnetization diagram of Co@PCL17 (dotted), Co@PCL23 (dashed), and Co@PCL32 (solid) in toluene.

mass of ca. 4.7×10^{-18} g (with $d_c = 10$ nm, $\rho_{Co} = 8.9$ g·cm^{-3}) and an average surface area of ca. 300 nm^2, this corresponds to 600 chains per particle or 2 chains per squared nanometer.

Additional and complementary information on the size of the core and shell of the hybrid particles can be obtained from transmission electron microscopy (TEM) and atomic force microscopy (AFM), respectively. As shown in Figure 3a, spherical objects are detected in AFM experiments with an average diameter of 30.3 ± 4.5 nm for Co@PCL27 which is in good agreement with DLS results (see Table 1). The shell is supposed to be stretched out in AFM experiments due to solvation with xylene (a good solvent for PCL). In contrast to this, the polymeric shell is collapsed in samples prepared in the dry state for TEM experiments (see Figure 3b). The average core diameter determined by TEM is 9.8 nm ± 1.4 nm (inner) and 12.9 nm ± 2.1 nm (outer diameter), respectively.

Quasi-static Magnetic Properties. In vibrating sample magnetometry (VSM) experiments, the magnetization of a sample is recorded against the applied magnetic field strength in order to gain information on the response of the sample to a quasi-static and homogeneous field. The equilibrium properties of the magnetic dispersions give information on the core properties and concentration and should not be influenced by the presence of a polymeric shell, provided that the particles are well-dispersed and able to rotate freely. Information is gained on the saturation magnetization M_s of the sample by extrapolation of the magnetization, M, to an infinitely strong magnetic field $H \rightarrow \infty$ and on the volume-average magnetic moment m_v of the involved particles from the respective initial susceptibility obtained from the initial slope of the graph (see Figure 4).

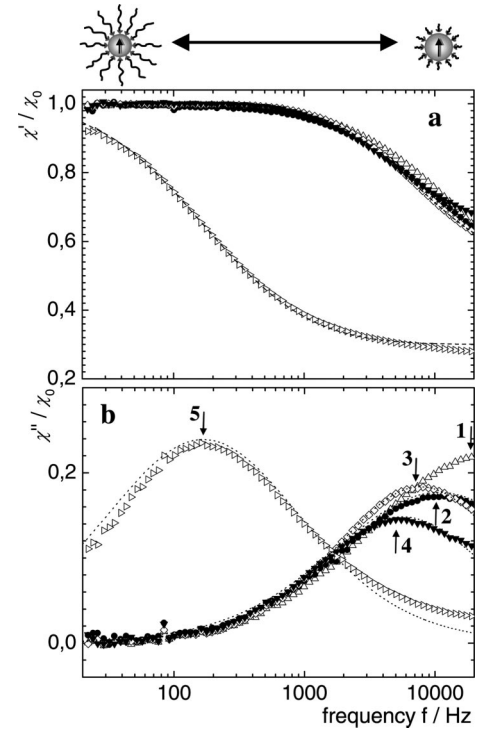

Figure 5. Results for the frequency dependence of χ'/χ_0 (a) and χ''/χ_0 (b) from AC susceptometry analysis and best fits for Co@RA (open upright triangles, **1**), Co@PCL17 (filled circles, **2**), Co@PCL23 (filled downward triangles, **3**), Co@PCL27 (open rhombs, **4**), and Co@PCL32 (open sideward triangles, **5**).

The saturation magnetization increases with shell thickness indicating a higher Co content, possibly due to a more effective stabilization of the highly interacting magnetic particles by steric repulsion of the brushes. Magnetic fluids

(40) Frait, Z.; Ondris, M. *Czech. J. Phys.* **1961**, *11*, 463.

Table 2. Dynamic Magnetic Properties of the Hybrid Co@RA and Co@PCL Core−Shell Particles

run[a,b]	d_v (nm)	η (cP)	f_{char} (Hz)	$d_{h,AC}$ (nm)	σ	SHP (W·g^{-1})
Co@RA	17.2	0.55	19100	nd	0.45	346.6
Co@PCL13	22.1	0.56	nd	nd	nd	nd
Co@PCL17	25.2	0.59	11000	18	0.46	299.3
Co@PCL23	26.3	0.64	8000	28.5	0.29	282.8
Co@PCL27	30.9	0.67	5500	35	0.31	186.3
Co@PCL32	38.5	0.70	170	58	0.5	50.2

[a] d_v: volume-average hydrodynamic diameter, from DLS. η: viscosity. f_{char}: characteristic frequency. $d_{h,AC}$: volume average hydrodynamic diameter, from AC susceptometry fit. σ: standard deviation of ln $d_{h,AC}$, from AC susceptometry fit. SHP: specific heating power at 300 kHz. [b] Nomenclature: Co@RA ricinolic acid functionalized cobalt nanoparticles; Co@PCL*xy* cobalt nanoparticles with a poly(ε-caprolactone) brush shell; $xy = M_n/100$.

with a saturation magnetization M_s of up to 3.7 kA·m^{-1} were obtained. Assuming single crystal ε-Co cores ($M_0 = 1{,}46 \times 10^6$ A·m^{-1}),[40] the cobalt content of the dispersions, $\mu_{Co,disp}$, is calculated to be up to 2.8 mass % (0.3 vol %), thus considerably below magnetic or hydrodynamic interaction. The initial susceptibility χ_{ini}, that allows the calculation of the average involved magnetic moments, is extracted from the initial slope of the graph, and values in the range of $7.3-7.9 \times 10^{-19}$ A·m^{-1} are found, giving volume-average diameters d_c of the respective cobalt cores in all samples that are in good agreement with observations from TEM and with the values determined for unfunctionalized cores (Table 1).

Dynamics of the Particle Rotation Examined by AC Susceptometry. In contrast to the quasi-static magnetic properties, the behavior of magnetic colloids in dynamic magnetic fields is ruled by the response rate of the particles related to the alternating field and is strongly dependent on its frequency. Due to theoretical considerations,[41] cobalt nanoparticles with a diameter of 8 nm and higher are magnetically blocked, i.e., the direction of the collective magnetic moment of the single-domain particles is blocked along the direction of the easy axis of the crystallite due to the intrinsic anisotropy of the particles (Figure 1). Therefore, as the particle is exposed to a high-frequency electromagnetic field, magnetization reversal is only possible by particle rotation. The covalently attached polymer brush shell is involved in the rotation, and the crucial parameter is the hydrodynamic diameter of the particle in dispersion. Thus, the rotational characteristics of the presented nanorotors are supposed to be dominated by a shell thickness effect. In order to verify this strategy, the dynamic magnetic properties of the particles were analyzed by AC susceptometry.

The method gives information on the rotational diffusion of the core−shell particles by the determination of the frequency dependence of the magnetic susceptibility. The applied frequency range corresponds to the expected time scale of Brownian rotation for the investigated particle batches with hydrodynamic diameters d_h between 22 and 39 nm (DLS, Table 1), estimated from eq 1. A weak alternating magnetic field induces a harmonic change in the magnetization M so that the dynamic magnetic susceptibility χ can be defined as the ratio of M to the magnetic field strength H:

$$M = \chi H \tag{3}$$

The frequency-dependent susceptibility, χ, can be split into a real (in-phase) part χ' and an imaginary (out-of-phase) part χ'':

$$\chi(\omega) = \chi'(\omega) - i\chi''(\omega) \tag{4}$$

Following Debye's theory,[42] the real and imaginary parts' dependencies on the frequency ω are given by

$$\chi'(\omega) = \frac{\chi_0}{1 + (\omega\tau)^2} \tag{5}$$

and

$$\chi''(\omega) = \chi_0 \frac{\omega\tau}{1 + (\omega\tau)^2} \tag{6}$$

χ_0 represents the static susceptibility of the system. For the given experimental situation, the characteristic time τ is the Brownian relaxation time τ_B (eq 1). In practical MNP samples, the distribution of particle sizes has to be taken into consideration. In order to compare the results with those from dynamic light scattering measurements, we consider a log-normal volume distribution $f_V(d_h)$ of particle diameters.

$$f_V(d_h) = \frac{1}{\sqrt{2\pi} d_h \sigma} \exp\left[- \frac{\ln^2(d_h/\bar{d}_h)}{2\sigma^2} \right] \tag{7}$$

where $\bar{d}_h$ is the median hydrodynamic diameter, and σ is the standard deviation of ln d_h.

In the present case, it is necessary to account for the different contributions of shell and magnetic core to the relation between hydrodynamic diameter and the frequency-dependent susceptibility signal, as pointed out by Chung et al.[43] In particular, while only the core volume contributes to the susceptibility, the shell determines the hydrodynamic properties. Thus, the model includes a different weighing for d_c and d_h. By implying that the distribution of the hydrodynamic particle diameter is dominated by a log-normal distribution of the Co cores and that the relaxation time is dominated by the Brownian relaxation, thus $\tau = \tau_B$, and finally by replacing the number-weighed log-normal distribution of Chung et al.[43] by the volume-weighed one used in eq 7, we obtain an expression for the frequency dependent susceptibility in terms of an integral over the hydrodynamic particle size distribution;

$$\chi'(\omega) = \chi_0 \int_0^\infty \frac{d_c^6}{d_h^3} \frac{f_V(d_h)}{1 + (2\pi\eta\omega d_h^3/(kT))^2} \, \mathrm{d}d_h \tag{8}$$

and

$$\chi''(\omega) = \chi_0 \int_0^\infty \frac{2\pi\eta\omega d_c^6 f_V(d_h)/(kT)}{1 + (2\pi\eta\omega d_h^3/(kT))^2} \, \mathrm{d}d_h \tag{9}$$

The AC susceptometry results for Co@RA and Co@PCL dispersions in toluene are presented in Figure 5 for a frequency range of 20 Hz to 20 kHz at a field amplitude of

(41) Puntes, V. F.; Krishnan, K. M. *IEEE Trans. Magn.* **2001**, *37*, 2210.

(42) Debye, P. *Polar Molecules*; Chemical Catalog Company: New York, 1929.

(43) Chung, S.-H.; Hoffmann, A.; Guslienko, K.; Bader, S. D.; Liu, C.; Kay, B.; Makowski, L.; Chen, L. *J. Appl. Phys.* **2005**, *97*, 10R101.

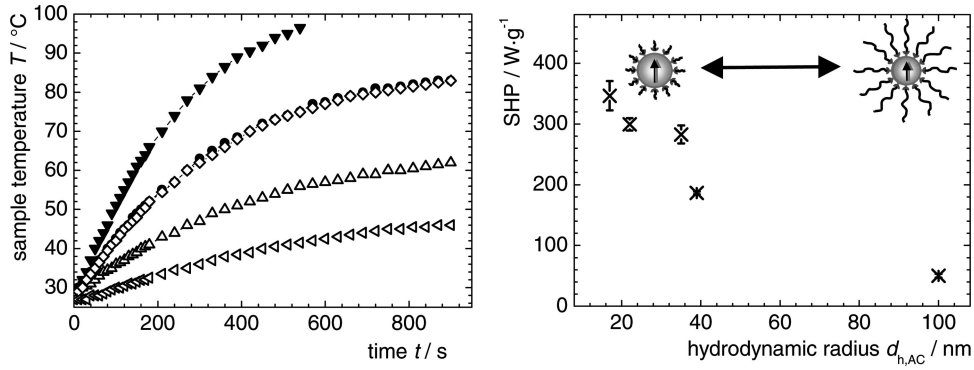

Figure 6. Magnetic heating results for Co@RS and Co@PCL samples. (right) Sample temperature vs time. (left) SHP vs hydrodynamic diameter. See Figure 5 for more information about the progression shown inset in the graph.

0.25 mT. A maximum in the imaginary part of the susceptibility is detected in the studied frequency range for all investigated samples, except for the sample Co@RA with the smallest hydrodynamic diameter of 17 nm (DLS, Table 1). The measurements were fitted using eqs 8 and 9 for χ' and χ'', taking into account the samples viscosities η as obtained from Ostwald viscosimetry.

As can be seen from Figure 5, the real part χ' does not drop to zero at high frequencies even for particles with the highest hydrodynamic diameter Co@PCL32 (as theoretically expected for single-mode relaxation) but levels off at a finite value, in contrast to the imaginary part. This may be the result of a small fraction of hybrid particles with a core below the critical diameter for blocked particles and is taken into account in the calculations.

The characteristic frequency f_{char} at maximum loss and the parameter values for $d_{h,AC}$ and σ obtained from the best fit are given in Table 2. For most systems, satisfactory agreement is obtained between the volume-weighted hydrodynamic diameter values $d_{h,AC}$ obtained from AC susceptometry measurements and d_v values obtained by DLS. These data show the expected trend, indicating a distinct effect of particle thickness on the dynamic magnetic properties of the hybrids and thus verifying the hydrodynamic (rotational) nature of response to the field.

However, for particles with a thicker shell (Co@PCL32), considerable deviation is observed. Possible explanations for the deviation are based on differences between DLS and AC susceptibility measurements. The former one is determined by the translational diffusion, while the latter method is ruled by the rotational movement of the particles. A similar observation on electrostatically stabilized $CoFe_2O_4$ ferrofluids has been interpreted to be due to the existence of small agglomerates in the case of translational diffusion.[20]

Furthermore, the analysis of the DLS and susceptibility data are based on the assumption of rigid spherical particles and boundary conditions determined by the Stokes−Einstein and Einstein expressions for the translational and rotational thermal motions respectively,[15,16] not taking into account the flow field modification stemming from the internal friction of the brushlike shell under shear.[4446] The effect of tethered polymer brushes on the flow field and the apparent slip near the surface have been addressed theoretically and experimentally before,[47–50] albeit mostly in relation to planar surfaces. Thus, it is reasonable to identify another possible source of deviation resulting from the increased tendency for a shift to "slip/no slip" boundary conditions with increasing grafted polymer chain length.[46] This latter explanation is further supported by the increase in viscosity with particle size. The detailed study of this possibility is beyond the scope of the present work and will be examined in detail in future work.

Nevertheless, it is obvious from the data, that the characteristic frequency of the particles, i.e., the frequency at which the maximum in χ'' occurs, is altered by the influence of the shell thickness, while the response to static fields as indicated by VSM measurements occurs from individual cobalt cores.

Magnetic Heating Capacities of Particle Dispersions. The field-induced particle rotation impacts the magnetic heating behavior of particles when exposed to an alternating field in the radio frequency range due to the internal friction of the rotating particles. This is shown by exposure of the samples to an AC field with fixed frequency at 300 kHz, thus well above of the characteristic frequency of the particles. In this regime, the particles are forced to a rotation limited by their hydrodynamic radius, thus the particle radius is of impact on the heat evolution observed under irradiation. In order to investigate this, the temperature of the fluids is recorded against time, giving information on the specific heating power (SHP) of the particles from the initial slope dT/dt of the graph and the specific heat capacity c_p.

$$\mathrm{SHP} = \frac{c_p}{\mu_{\mathrm{Co,disp}}} \cdot \frac{\mathrm{d}T}{\mathrm{d}t} \tag{10}$$

The resulting temperature profiles are shown in Figure 6 together with the obtained SHP values for the different samples. The fluids show a considerable temperature rise

(44) Pelletier, E.; Belder, G. F.; Hadziioannou, G.; Subbotin, A. *J. Phys. II France* **1997**, *7*, 271.
(45) Kumaran, V. *Macromolecules* **1993**, *26*, 2464–2469.
(46) Doyle, P. S.; Shaqfeh, E. S. G.; Gast, A. P. *Macromolecules* **1998**, *31*, 5474.
(47) Halperin, A.; Tirrell, M.; Lodge, T. P. *Adv. Polym. Sci.* **1992**, *100*, 31–71.
(48) Semenov, A. N. *Langmuir* **1996**, *11*, 3560–3564.
(49) Nommensen, P. A.; Duits, M. H. G.; van den Ende, D.; Mellema, J. *Phys. Rev. E.* **1999**, *59*, 3147.
(50) Wyart, F. B.; de Gennes, P. G. *Eur. Phys. J. E* **2000**, *1*, 93–97.

within minutes, depending on the cobalt content of the fluids and their respective heating capacities. While the cobalt concentration in the fluids increases with shell thickness according to VSM (Table 2), the specific heating power decreases, resulting in the observation that the heat development of the different species, indicated by initial dT/dt, passes through a maximum for Co@PCL23 (Figure 6 right panel).

From the relation of the SHP on the mean hydrodynamic diameter values obtained from AC susceptometry, it is found that the faster the particles are able to rotate, the higher is the amount of the heat generated. This is in accordance with the above considerations. However, the relationship is not linear, as would be the case if the heating power of a single rotation is constant for the investigated particles. In contrast to this, the SHP/f ratio is increasing with shell thickness. Future experiments will give more insight into the impact of the shell and internal friction on the heat evolution and transfer of such systems.

Conclusions

Decorating blocked magnetic Co particles with a poly(ε-caprolactone) shell of adjustable thickness results in magnetically activated nanorotors with an angular speed limited by the hydrodynamic properties of the shell. The hydrodynamic nature of the magnetization reversal is investigated by AC susceptometry and in terms of magnetic heating. Fitting of the AC susceptometry experimental data according to Debye's theory assuming a log-normal distribution of hydrodynamic diameters leads to particle sizes that in most cases are comparable to DLS results. In magnetic heating experiments, we observe AC losses at a frequency well above the characteristic frequency by recording the sample temperature and find decreasing loss values for bigger particles at a constant frequency as theoretically expected.

The presented results show how rotational actuation can be activated in blocked single domain magnetic nanoparticles and that the behavior can be tailored to a certain frequency by a polymer shell. The materials may be of interest for microfluidic transport or mixing systems in laboratory-on-a-chip applications.

Acknowledgment. We thank Sylvio Dutz, IPHT Jena (VSM), Filip Oesterheld, HHU Düsseldorf (AFM), and Silke Behrens, FZ Karlsruhe (TEM), for analytical assistance and Nina Matoussevich for providing the cobalt nanoparticles. Financial funding is acknowledged from DFG (Emmy Noether Program and SPP 1104). Thanks go to Helmut Ritter and Moshe Gottlieb for fruitful discussions.

CM703419T